American Journal of
Oral Medicine and Radiology

ISSN - 2394-7721

www.mcmed.us/journal/ajomr

Research Article

A INFORMATION FUSION BETWEEN PHYSIOLOGY AND ANATOMY APPROACH TO RESTORING IMAGES OBTAINED WITH SPECT-MRI

Dr. Prakash kulithungan[1]*, Dr. Revanth V[2]

[1]Associate Professor, Sri lakshminarayana Institute of medical sciences, Puducherry
[2]Assistant Professor, Sri lakshminarayana Institute of medical sciences, Pondicherry

ABSTRACT

Image restoration in image processing is often Because of its ill-posedness to the lack of specific solutions. An image's quality is significantly affected by the limitations imposed by the solution's characteristics. In this study, To enhance the restoration of NAS-RIF, we propose an extension with use in SPECT medical imaging based on data fusion. In the NAS-RIF approach, the restoration process can be restricted by adding a regularisation term that stabilises the inverse solution. In anatomical restoration techniques (MRI), high resolution data can limit the restoration process. A structural anatomy-based regularisation term is created by unsupervised Markovian segmentation based on the volume of Data collected by patients through MRI and SPECT. As part of the evaluation, thirty pairs of MRIs and SPECTs were acquired were performed on various individuals and phantoms from Hoffman and Jaszczak. The signal-to-noise ratio is the number of signals per unit of noise, the method outperforms a traditional Metz filter-based guided restoration strategy.

Key words:- MRI, SPECT-MRI, NAS-RIF, Metz filter-based guided restoration

Access this article online		
Home page: http://www.mcmed.us/journal/ajomr	Quick Response code	
Received:25.10.19	**Revised**:12.11.19	**Accepted**:14.12.19

INTRODUCTION

This poorly posed inverse problem requires the inclusion of a regularization term in the picture restoration framework. Using this fusion-based regularisation term, we explore any challenges associated with picture restoration when data from a different modality is used (intermodality). Our present study focuses on a novel modification It is possible to constrain NAS-RIF inverse filtering using an intermodality registration, which enables NAS-RIF inverse filtering to be computed, by configuring the NAS-RIF inverse filtering with the Surgical images that require restoration of anatomical and functional information (from the same anatomical structure).

Corresponding Author
Dr. Prakash kulithungan

A high spatial resolution Imaging procedure, such as CT scans or MRIs, can help determine our application to extract anatomical information, and the high spatial resolution mode is then utilized in functional SPECT imaging to improve contrast.

Single photon emission computed tomography (SPECT) images of the brain exhibit high contrast and a high signal-to-noise ratio are somewhat In comparison with anatomical dimensions approaches of imaging (The use of MRIs and CT scans). Thus, SPECT images of the brain can provide information about only be used in a limited number of applications. A functional deficiency, on the other hand, has a significantly lower tracer uptake than focal atrophy, whose tissue is physically intact but whose CSF replaces it [1].

Images taken with SPECT have a high spatial resolution has been enhanced by a number of techniques to date. Techniques used to restore images can be divided into two main categories: those that utilize the restoration techniques that are used during reconstruction from projections, as well as those that are used after the reconstruction has been completed. We provide a method for Reconstruction after post-tomography that is largely independent of scanner characteristics in this study.

For example, Rajabi et al. used four commonly Filters used (Hannaning, Butterworth, Metz, and Wiener) for investigating SPECT of the myocardium with Tc-sestamibi perfusions [2]. Hatzinakos and Kundur [4] introduced NAS-RIF to accommodate an imaging method based on 3D SPECT in [3] in order to restore the context for 3D SPECT imaging. When An object's image is blind deconvoluted with NAS-RIF a gray (or noisy) backdrop, the method is applicable. Since an image Against a noisy background, a finite support represents an actual, unaltered rCBF map of the human brain, this technique can be effectively used for brain SPECT imaging (the background depends on Radioactive imaging is subject to both Poisson noise and on electronic noise from a scanner), this technique can be used effectively for brain SPECT imaging. This deconvolution technique only requires the nonnegativity of the genuine image as well as its support. According to [3], a 3D Markovian segmentation method was used to correctly identify this support using the SPECT volume.

In the Bayesian tomographic reconstruction process [5, 6], the same tactic is used Without smoothing edges, noise can be controlled, but in this case during the reconstruction process. Anatomical "landmarks" are identified by In addition to structural information regarding these landmarks, the presence and location of local discontinuities and homogeneous regions can be gathered as well, as shown by MR images). The models usually suggest that adjacent Functioning pixels should have the following characteristics: a gray level value of the same value There are two types of homogeneity: a local (local homogeneity) and a global (global homogeneity) Anatomically segmented and recognized "uniform" areas.

By adding spatially-adapted regularization to the NAS-RIF algorithm, we propose extending the approach described in [3]. In addition to minimizing noise amplification and ringing aberrations, this regularisation term integrates anatomical information derived from high-resolution anatomical MRI images efficiently [9]. After registering the patient's MRI and SPECT volumes, the unsupervised Markovian segmentation output was acquired via this structural anatomy-based regularisation term. Because the proposed regularization term is quadratic, the NAS-RIF process minimises a newly convex objective cost function using recursive filtering of the degraded image. A supervised deconvolution/restoration procedure using a traditional Metz filter was used to evaluate our restoration technique using Hoffman and Jaszczak SPECT Phantoms.

Following is a breakdown of the essay's structure. Section 2 briefly describes the NAS-RIF 3D anatomical constraint deconvolution method. Described in Section 3 are the algorithms for registration and segmentation. A description of the validation procedure is provided in Section 4. Using phantom and actual brain SPECT volumes, we then validate the suggested model in Section 5. Our discussion comes to an end in Section 7.

In NAS-RIF, anatomical restrictions are imposed Version D of the Extended NAS-RIF

Using the linear model proposed in [3], we assume that 3D SPECT images will be degraded in our application. The operator and the additive noise represent the true image and the point spread function (PSF), respectively, as well as the 3D discrete linear convolution operator. In other words, the 3D blind deconvolution problem asks the observer to figure out (or its inverse) in the face of hazy observations.

The 3D extended version of the NAS-RIF deconvolution algorithm uses the output of a FIR filter of dimension to estimate the true image. An estimated 3D image is then projected using a nonexpansive mapping (implying that the image is assumed to be nonnegative and has a known support) using a nonlinear filter that assigns the estimated 3D picture to a space corresponding to the known properties of the genuine image. This difference between this projected image and is the error signal for updating the variable filter. 3D deconvolution cost functions are defined as where, if, and if for the deconvolution of 3D images. Each pixel inside the support zone is represented by a single pixel, and each pixel outside the support zone is represented by a single pixel.

Using the first term, negative voxels in the support are penalized in order to keep the image estimate nonnegative. In cases where coordinates outside of the support differ significantly from those in the background average, the second term penalises them. In this case, a positive constant is used to avoid a simple all-zero minimal solution.

With respect to the 2D case, the above equation is convex, as described in [10]. A similar characteristic applies to convergent gradient minimization in a 3D situation, enabling the algorithm to reach a global minimum through conjugate gradient minimization [10].

3D Anatomical Constraints for NAS-RIF

One of the main drawbacks of the NAS-RIF technique is that it amplifies noise at low SNRs [4]. The high-pass characteristic of the inverse filter amplifies high-frequency noise, leading to this effect. Therefore, the solution at convergence could not provide the most accurate estimate of the actual item in the presence of

noise. [4] Kundur and Hatzinakos suggest stopping the iterative restoration process through eye examinations as a solution to this issue. Due to strong supervision required and the difficulty in identifying the best iteration for termination (different parts of the image can converge at differing rates), this method is unreliable in reality.

NAS-RIF can be augmented with anatomical data from MRI (or CT) images with high resolution by using this regularisation method in this study. Besides preventing noise amplification, the proposed regularisation term stabilizes the inverse solution, does not require supervision (parameter tweaking or stopping criteria), and can provide more effective constraints to the restoration problem. To recover this functional SPECT image across previously discovered and segmented anatomical regions, a piecewise smoothness restriction must be applied. This can be achieved by combining the output of both an initial registration step between the MRI and SPECT images and a segmentation step between the MRI image and the anatomical class we are interested in.

There are three main "anatomical" types (tissues) found in the brain: white matter (), gray matter (), and cerebro-spinal fluid (). As a result of our model, we have defined the new cost function for deconvolution of the 3D image as follows: where the first summation is taken from these three anatomical types (tissues) and designates the mean, in gray levels, of the ith region, and is used to weight these anatomical constraints. For each spectra of the SPECT picture, voxels are proportional to variance within each anatomical region for each transverse slice. Within a recognized and segmented anatomical region, pixels in a functional image usually have the same gray level values. Edge-preserving regularisation is possible with this regularization term since it enables smoothness constraints to be applied without removing (anatomical) discontinuities.

This regularisation component does not change the convexity of the NAS-RIF cost function, ensuring a unique solution to the problem. According to Figure 2, this scheme is framed within a framework. This function calculates the cost of a SPECT scan using (high-resolution) MRI data with the result of dividing the MRI volume into anatomical classes.

(7) shows the first derivative of the cost function. Every entry is written as follows: With respect to, the gradient vector is:

A gradient-based iterative restoration procedure can be used to minimise this convex cost function. Due to the quadratic nature of the suggested criterion, alternative optimization techniques can be applied as well.

NAS-RIF algorithm requires the Kronecker delta function [10] as its first inverse FIR filter. Also, our choice was based on the fact that the background of the SPECT image is not entirely black [4].

We define the final convergence condition of the proposed algorithm as the stability of the cost function minimization, where is a threshold commonly used in our application, and where n represents the number of iterations. Using the gradient descent procedure in Figure 8, a change in the cost function value is depicted in Figure 3.

Anatomically based regularisation is defined using a 3D registration step between MRI and SPECT input volumes (from the same patient) [11, 12], followed by a Markovian segmentation of the MRI 3D image into anatomical classes [9]. The following sections describe the process (see Section 3.2.).

Segmentation and enrollment

Our anatomically based regularisation term is defined by unsupervised Markovian segmentation of the (registered) MRI 3D picture into anatomical classes using the result of the 3D registration step between the MRI and SPECT input volumes.

Enrollment

In [12], we explain how we used mutual information to register 3D objects in our application. As the maximum value of MI registration criterion between MRI and SPECT volumes specifies the amount of information in the joint histogram of the images, it produces the best match of intensity correspondences between the images for registration. Maximising [13] is used to discover the best set of registration parameters, after estimating the vector using Powell's method. In order to speed convergence, the cost function is slightly smoothed, which will decrease the likelihood of finding undesirable local minima (due to incorrect registration). The code used to register the MR picture with the SPECT picture was heavily influenced by the software program Statistical Parametric Mapping (SPM)[14]. (View Figure 7.)

A method for segmenting the volume of an MRI

This involves using two random fields, where represents the label field and represents the field of observations on the 3D lattice of sites (voxels) associated with class labels of segmented 3D images. There are three categories of brain "tissue" labeled above, each corresponding to an area of the 3D brain image. Tissues that absorb no trace amounts of a tracer are grouped together with CSF and extra-cerebral tissues. Although there is nonzero tracer presence in the skin and other external structures (there is blood flow), we believe it has no practical significance. It is the CSF area (intracerebal ventricles and peri-cerebral cysterns) that refers to the immediate environment of the brain and areas that are genuinely unresponsive. Gray matter (the brightest area) and white matter (the dullest area) have different patterns of blood flow [15]. There is a value for each (grey levels), and there is a value for each (white levels). The distribution of (designates the gray level intensity associated with the site) is defined using a prior

distribution assumed to be Markovian and site-wise conditional likelihoods.

During the estimation process, there are several steps

The likelihood of the sample is estimated using three Gaussian laws and the Iterative Conditional Estimation (ICE) technique [16].

A markerovian segmentation of the MR volume can be calculated unsupervised using estimates provided by the ICE process. As an example of a global Bayesian formulation of a statistical labeling problem, Markovian segmentation can be viewed as maximizing the posterior energy [17]: expressing the adequacy between observations and labels and representing the energy of the a priori Pott model (which tends to favor homogeneous regions without privileged orientations). A deterministic Iterated Conditional Modes (ICM) algorithm is used to reduce this global energy function. ML segmentation is used as the initialization for this approach, which uses the segmentation map produced by ML. A support value is then calculated based on pixels belonging to the CSF, white matter, and gray matter classes. The figures 5 and 6 illustrate this point.

Authentication

A method for acquiring and reconstructing SPECT data

We captured the SPECT images with a triple-he ad gamma camera (Picker Prism, Cleveland, OH, USA) u sing low-energy, high-resolution parallel-hole collimators . A 360° field of view was obtained by obtaining SPECT projections every few seconds. Ethylene Cysteinate Dime r (TC-ECD) was used as the radioisotope.

Data collection for MRIs

An MRI picture was obtained using a 3D-FISP o n a Siemens Magnetom Avanto T scanner. The excitation method used was nonselective. There were 512 512 voxel s per slice and TR = ms, TE = ms, and scanning paramete rs were TR = ms, TE = ms, and. We further processed the 3D MRI images by varying BET's fractional intensity thr eshold to separate the brain from other tissues using the b rain extraction tool (BET) [18] of the MRI programme.

Prototype Validation Protocol for Phantom

A total of two imaging phantoms were used to te st the efficiency of our SPECT image restoration techniq ue (i)

SPECT imaging was used to scan the Hoffman 3D Brain Phantom [19] while it was carrying MBq of activity. To match as closely as possible the MRI image's slice orient ation, the phantom was oriented according to its slice orie ntation. Data from phantom SPECT included slices with voxel dimensions of . An MRI Phantom data set contains mm isotropic voxel slices. An illustration of the Hoffman phantom's transversal slices is given in Figure 1. A spher e of varying diameters (diameters 1, 2, 3, 4, 5, and 6 mm) composes the other phantom. Spheres filled with a radioa ctive solution were compared with a less concentrated rad ioactive solution present in background in one scenario, r esulting in an activity concentration ratio of approximatel y. A low-activity solution was used in the cylinder, and n onradioactive water was used in the spheres. Data from th e phantom SPECT showed the following voxel dimensio ns. Slices of isotropic mm-sized voxels were included in t he Phantom MRI data. Figure 1 [20] shows transaxial slic es of the phantom (Deluxe ECT).

Despite being a quick and easy means of assessing the effectiveness of a technique, visual inspection is obviously an inadequate measurement. Based on the improvement in signal-to-noise ratio (ISNR), measured in decibels (dB), the degraded phantom image, the ground truth and restored phantom images are used to calculate the performance metric. In this case, the restored phantom image corresponds to the quadratic norm. Based on the ISNR, we can calculate the reflection coefficient by adding the degraded phantom picture, the original (ground truth) phantom image, and the restored phantom picture. In our case, the original object was the MRI phantom, and each compartment's radioactivity concentration was also known; therefore, this measure is only useful if the original object is known.

A unique evaluation criteria from [22, 23] was also applied to restore images based on the assessment of the four following parameters.

In the white and gray matter regions, and are the means of the pixel values, respectively, for the image's overall contrast [22].

Using the mean gray level value inside the sphere and the mean gray level value outside the sphere (in a circle centered around the sphere and whose radius equals half the distance between the centers of the spheres in the image), one can define the local contrast of the picture [23].

As shown in [22], the white matter region represents the standard deviation of pixel values within this region.

As a final example, we can take a look at the mottle in the gray matter region of the image [22], defined as, where the standard deviation of the pixel values in this region is (iv).

In a consistent area of the SPECT volume, these two measurements can be used to assess whether noise has been amplified and/or if unwanted artefacts have been introduced by the restoration process. Total mottle was calculated by adding pixels from white and gray matter areas, respectively, to calculate the percentage of pixels in each. Each category of brain anatomical tissue has a different number of pixels. An effective SPECT image restoration technique improves image contrast while minimizing mottle. Alternatively, we can determine if contrast enhancement was significant for a particular maximal mottle measure [22].

Supervised Metz Restoration Filter compared to the evaluation

By comparing our method to the traditional Metz filter deconvolution method, we were able to demonstrate the advantages of this unsupervised, blind deconvolution method [24]. In order to restore images using Metz filters, you need to understand the point spread function (PSF) of the imaging system. Inverse filtering and low pass filtering are combined in the filter. By using this filter, it is possible to deconvolve SPECT images while decreasing extremely high frequencies (i.e., noise caused by inverse filtering). Metz filters have two parameters that can be adjusted: their size and their order (full width at half maximum).

Results of the experiment

The clinical data from 30 epileptic patients' MRI and SPECT scans were restored. In each set of SPECT data, voxel slices had the following dimensions: and. Data sets with MRI showed slices of voxels with voxels of size. In this section, several examples are provided from this category.

MRI technology was used to separate the brain from other tissues before registration and restoration. Fractional intensity threshold for BET was set at. The empirical selection of this value was based on visual assessments of a number of test runs.

In Figure the ISNR variance of processed phantom pictures is illustrated for a variety of FWHM parameters as well as for the optimal value. FWHM = mm or ISNR dB was found to be the best restoration value based on ISNR comparisons for various FWHM values.

The average contrast and total mottle were first quantified and compared with the Metz filter on a collection of (human brain) degraded and restored SPECT images. The suggested approach led to an increase in mottle and global contrast with the appropriate factor. By boosting global contrast and mottling by and respectively, the Metz filter boosted global contrast and mottling.

In Table 1, you will find comparable results for SPECT phantoms. We selected the weighting factor for the studies we examined because SPECT images do not have a completely black backdrop [4]. A series of tests was conducted to determine this value, then the interval was altered to arbitrarily select it.

Table 1: Using the restored image with or without, the Metz filter, and the original phantom SPECT, they compute the global contrast and mottle (expressed in %), as well as the improvement in signal-to-noise ratio (expressed in dB).

		with $J_4(u)$			Metz filter			without $J_4(u)$			
	C_G	M	$ISNR$	C_G	M	$ISNR$	C_G	M	$ISNR$	C_G	M
Hoffman	29.5	26.3	0.720	24.0	21.1	0.421	20.3	18.9	0.299	18.3	18, 4
Cold spheres	27.3	37.5	0.679	21.8	33.4	0.399	20.6	27.6	0.241	18.1	27.1
Hot spheres	28.9	39.8	0.670	21.2	34.2	0.386	20.1	28.5	0.227	17.4	27.5

Table 2: Anatomical contrast (expressed in %) obtained from the restored image with and without the correct anatomical information

Cold Sphere$_i$	1	2	3	4	5	6
CL (with partial anatomical errors)	23.8	21.1	18.4	15.7	11.7	6.7
CL (with anatomical information correct)	24.4	20.6	16.9	15.9	10.5	7.9

Table 3: Local contrast (expressed as a percentage) with the correct anatomical information obtained from restored and degraded phantom SPECT images, respectively.

		Restored images		Degraded
Cold sphere	with $J_4(u)$	Metz filter	withou t $J_4(u)$	image
	C_L	C_L	C_L	C_L
1	24.4	18.2	17.1	15.4
2	19.6	17.7	15.9	13.1
3	16.9	13.3	12.2	10.3
4	15.8	11.4	10.0	8.8
5	10.4	8.1	7.0	5.1
6	7.9	5.6	4.1	3.1

Figure 1:
Phantoms sliced transaxially. An MRI with a Hoffman phantom (a). A Hoffman phantom SPECT is shown in (b). Phantom cylindrical MRI (c). SPECT with hot spheres on a cylindrical phantom (d). A cylindrical phantom MRI is shown in (e). An imaging technique involving cylindrical phantoms with cold spheres (f)

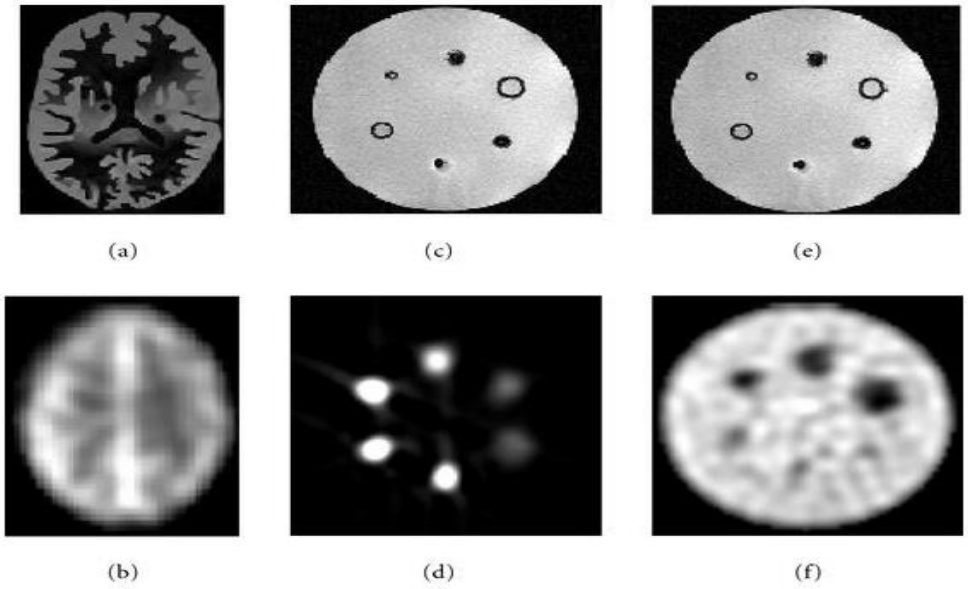

Examples of MRI cross-section images of human brains. From left to right: Original MRI cross-sectional images of human brains; and from right to left: Unsupervised three-dimensional Markovian segmentations.

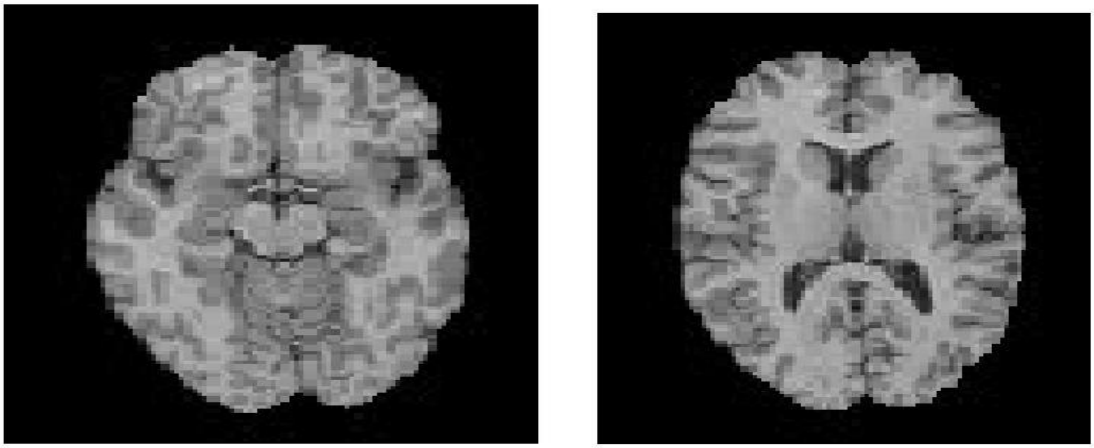

DISCUSSION

Using an experimenter to set the fractional intensity threshold, our restoration process was less susceptible to it (i.e., the contrast value remained stationary for when the threshold level changed from to). The parameter that produced the best results across all thirty pairs of MRI scans has been chosen as the best value.

As opposed to our restoration approach, which assumes that noise is additive, noise is actually a multiplicative Poisson process. As a result, it is striking to see the results when actual SPECT/MRI data is used. (Multiplicative) Poisson and (additive) Gaussian noise differences do not seem to significantly affect the effectiveness of the algorithm at high count levels. It is important to conduct clinical studies utilizing ROC analysis in order to accurately assess the effectiveness of this restoration technique. These clinical studies will be discussed in another medical article.

We were able to increase signal-to-noise ratio by more than doubling what could have been achieved with a Metz filter. In light of the improvements in global contrast, ISNR, and local contrast measurement, which improve the ability of SPECT to detect focal abnormalities, the small increase in motility is not that big of a deal. Moreover, while our prior knowledge steered the restored image, noise from deconvolution operations didn't amplify the restored image.

Based on a GHz PC workstation running Linux, our method took about minutes to compute versus minutes for the Metz filter. The computational complexity of our method despite not requiring a PSF parameter makes it unsupervised.

Spect rCBF trials require MRI scans, which are another disadvantage of our approach, but from a clinical standpoint, they are a real necessity for most participants. In order to ensure the accuracy of the final restoration, the registration process must be of high quality. You can also find several more highly accurate registration techniques in many more places.

CONCLUSION

A reliable restoration technique for SPECT pictures was presented in this article that incorporates anatomical and functional information. It should be useful to doctors interpreting 3D SPECT scans of the human brain to use this technique in order to improve the high quality of these images. A high-resolution image such as a CT scan (or an MRI examination) is used to determine each subject's anatomical details. The proposed constraint term allowed for the generation of a better constraint on the resolution of our restoration problem as well as stability of the inverse solution of the NAS-RIF method by preventing noise amplification. As soon as these terms were registered to the subject's SPECT volume, those homogeneous anatomical regions reported in the high-resolution MRI scan could then be reconstructed into the SPECT image. In a variety of SPECT/MRI couples, this technique was tested for its effectiveness and reliability. Because it is a data-driven method, this fully automated 3D blind restoration method can be used for a wide range of 3D SPECT tests.

REFERENCES:

1. P. Calvini, A. M. Massone, F. M. Nobili, and G. (2006). Rodriguez, “Fusion of the MR image to SPECT with possible correction for partial volume effects,” *IEEE Transactions on Nuclear Science*, vol. 53, no. 1, pp. 189–197,
2. H. Rajabi, A. Bitarafan Rajabi, N. Yaghoobi, H. Firouzabad, and F. Rustgou, (2005). “Determination of the optimum filter function for Tc99m-sastamibi myocardial perfusion SPECT imaging,” *Indian Journal of Nuclear Medicine*, vol. 20, no. 3, pp. 77–82,
3. View at: Google Scholar
4. M. Mignotte and J. Meunier, (2000). “Three-dimensional blind deconvolution of SPECT images,” *IEEE Transactions on Biomedical Engineering*, vol. 4, no. 2, pp. 274–281,
5. D. Kundur and D. Hatzinakos, “A novel blind deconvolution scheme for image restoration using recursive filtering,” *IEEE Transactions on Signal Processing*, vol. 46, no. 2, pp. 375–390,
6. G. Gindi, M. Lee, A. Rangarajan, and I. G. Zubal, (1993). “Bayesian reconstruction of functional images using anatomical information as priors,” *IEEE Transactions on Medical Imaging*, vol. 12, no. 4, pp. 670–680,
7. X. Ouyang, W. H. Wong, V. E. Johnson, X. Hu, and C. T. Chen, (1994). “Incorporation of correlated structural images in PET image reconstruction,” *IEEE Transactions on Medical Imaging*, vol. 13, no. 4, pp. 627–640,
8. S. Sastry and R. E. Carson, (1997). “Multimodality bayesian algorithm for image reconstruction in Positron Emission Tomography: a tissue composition model,” *IEEE Transactions on Medical Imaging*, vol. 16, no. 6, pp. 750–761,
9. J. Nuyts, K. Baete, D. Beque, and P. Dupont, (2005). “Comparison between MAP and postprocessed ML for image reconstruction in emission tomography when anatomical knowledge is available,” *IEEE Transactions on Medical Imaging*, vol. 24, no. 5, pp. 667–675,
10. S. Benameur, M. Mignotte, J. Meunier, and J. P. (2006). Soucy, “An edge-preserving anatomical based regularization term for the NAS-RIF restoration of SPECT image,” in *Proceedings of the 13th IEEE International Conference On Image Processing (ICIP '06)*, pp. 1177–1180, Atlanta, Ga, USA, October
11. D. Kundur and D. Hatzinakos, (1996). “Blind image restoration via recursive filtering using deterministic constraints,” in *Proceedings of IEEE International Conference on Acoustics, Speech, and Signal Processing (ICASSP '96)*, vol. 4, pp. 2283–2286, Atlanta, Ga, USA, May
12. A. Collignon, F. Maes, D. Delaere, D. Vandermeulen, P. Suetens, and G. Marchal, (1995). “Automated multi-modality image registration based on information theory,” in *Proceedings of the Information Processing in Medical Imaging Conference (IPMI '95)*, pp. 263–274,
13. W. M. Wells, P. Viola, H. Atsumi, S. Nakajima, and R. Kikinis, (1996). “Multi-modal volume registration by maximization of mutual information,” *Medical Image Analysis*, vol. 1, no. 1, pp. 35–51,
14. M. J. D. Powell, (1964) “An efficient method for finding the minimum of a function of several variables without calculating derivatives,” *Computer Journal*, vol. 7, no. 2, pp. 155–162,
15. http://www.fil.ion.ucl.ac.uk/spm.
16. D. C. Costa and P. J. (1991). Ell, *Brain Blood Flow in Neurology and Psychiatry*, Series Editor: P. J. Ell, Churchill Livingstone, London, UK,

17. F. Salzenstein and W. Pieczynski,(1995). "Unsupervised Bayesian segmentation using hidden Markovian fields," in *Proceedings of the 20th IEEE International Conference on Acoustics, Speech, and Signal Processing (ICASSP '95)*, vol. 4, pp. 2411–2414, Detroit, Mich, USA, May
18. J. Besag, "On the statistical analysis of dirty pictures," *Journal of the Royal Statistical Society*, vol. 48, pp. 259–302, 1986.
19. S. M. Smith, (2002). "Fast robust automated brain extraction," *Human Brain Mapping*, vol. 17, no. 3, pp. 143–155,
20. http://www.mdanderson.org/education-and-research/departments-programs-and-labs/labs/pet-development-laboratory/research/hotpet-human-camera/hotpet-brain-scan-images.html.
21. http://guillemet.org/irene/equipe4/fantomes.html.
22. M. R. Banham and A. K. Katsaggelos, (1997). "Digital image restoration," *IEEE Signal Processing Magazine*, vol. 14, pp. 24–41,
23. S. Webb, A. P. Long, R. J. Ott, M. O. Leach, and M. A. (1985). Flower, "Constrained deconvolution of SPECT liver tomograms by direct digital image restoration," *Medical Physics*, vol. 12, no. 1, pp. 53–58,
24. A. H. Vija, E. G. Hawman, and J. C. Engdahl, (2004). "Analysis of a spectosem reconstruction method with 3D beam modeling and optional attenuation correction: phantom studies," in *Proceedings of the IEEE Medical Imaging Conference (MIC '04)*, pp. 2662–2667, October
25. C. E. Metz and R. N. (cs1974). Beck, "Quantitative effects of stationary linear image processing on noise and resolution of structure in radionuclide images," *The Journal of Nuclear Medicine*, vol. 15, no. 3, pp. 164–170,

Cite this article:
Dr. Prakash kulithungan & Dr. Revanth V. An Information fusion between physiology and anatomy approach to restoring Images obtained with SPECT-MRI. *American Journal of Oral Medicine and Radiology*, 2019, 6(2), 51-58.